Electrical Power and Energy Systems 176 (2026) 111758

Contents lists available at ScienceDirect

International Journal of Electrical Power and Energy Systems

journal homepage: www.elsevier.com/locate/ijepes

Combined methodology of statistical knowledge and adversarial learning for few-shot renewable scenario generation

Ke Wang [a,*], Yinan Zhou [a], Yuanxing Xia [a], Jun Liang [b], Xiangkuan Wan [a]

[a] College of Electrical and Power Engineering, Hohai University, Nanjing 210000, China
[b] Power electronics with the School of Engineering, Cardiff University, Cardiff, United Kingdom

ARTICLE INFO

Keywords:
Few-shot scenario generation
Statistical knowledge
Conditional generative adversarial networks
Random noise

ABSTRACT

Scenario generation plays a critical role in short-term power system operations with high renewable penetration. Data-driven scenario generation typically requires extensive sample data, however, due to confidentiality constraints or limited historical records—such as those associated with extreme weather scenarios—only small datasets may be available, thereby making credible scenario generation challenging. This paper proposes a combined methodology that integrates statistical knowledge and adversarial learning for few-shot renewable scenario generation. Specifically, the framework incorporates statistical knowledge that captures historical fluctuations and power prediction errors, together with conditional generative adversarial networks (CGANs), to generate accurate and reliable day-ahead or intraday look-ahead scenarios. This approach enables exploration of more diverse regions within the data space, generates a broader range of samples, and compensates for the lack of diversity resulting from limited datasets (e.g., one month or less). Case studies are conducted on a provincial power grid in China with abundant wind power resources. Compared with the traditional CGAN, the proposed methodology, when implemented with appropriate parameter settings, improves the coverage of the generated scenarios without increasing the corresponding power interval width.

1. Introduction

The increasing penetration of renewable energy has introduced substantial operational challenges to modern power systems due to its inherent intermittency and volatility [1–3]. Accurate scenario generation plays a crucial role in short-term power system operation, as it characterizes renewable power time-series variability and directly influences the outcomes of short-term optimal scheduling in systems with high renewable penetration levels [4–7].

Renewable power scenario generation methods can generally be categorized into model-based statistical approaches and model-free deep learning approaches. Model-based methods typically assume that renewable power follows a predefined probability distribution derived from historical data and generate scenarios through sampling techniques such as Monte Carlo (MC) simulation [8,9]. For example, a probabilistic power flow method integrating the Nataf transform and Latin hypercube sampling has been proposed to address wind, solar, and load uncertainties [10]. A hybrid vine copula-based approach combining K-means clustering with C-vine and D-vine copulas has also been introduced to model dependency structures among multiple wind farms and generate correlated wind power scenarios [11]. However, such statistical methods often rely on strong prior assumptions regarding physical conditions and idealized probability distributions. In practice, wind speed is frequently modeled using a Weibull distribution and solar power using a Beta distribution. These simplified assumptions fail to fully capture the nonlinear and highly dynamic characteristics of actual renewable power outputs, which may result in low-quality or insufficiently representative scenarios.

With the rapid advancement of data-driven technologies, model-free deep learning approaches have gained increasing attention in scenario generation. Unlike statistical models, deep learning methods do not require explicit distributional assumptions. They exhibit strong nonlinear fitting capabilities and can effectively extract complex temporal patterns from historical data. Among these approaches, Variational Autoencoders (VAEs) and Generative Adversarial Networks (GANs) are widely adopted [12]. GANs, in particular, have become more prevalent due to their unsupervised learning nature, which eliminates the need for manual data labeling. For instance, Wasserstein GAN (WGAN) has been applied to generate wind and photovoltaic scenarios

* Corresponding author.
E-mail addresses: wangkehhu@hhu.edu.cn (K. Wang), ynzhou@hhu.edu.cn (Y. Zhou), eexyx@hhu.edu.cn (Y. Xia), liangj1@cardiff.ac.uk (J. Liang), wanxiangkuan_hhu@hhu.edu.cn (X. Wan).

https://doi.org/10.1016/j.ijepes.2026.111758
Received 5 October 2025; Received in revised form 27 February 2026; Accepted 5 March 2026
Available online 12 March 2026

Nomenclature

Sets and Indices

i	Index to the sample number, from 1 to I
τ	Index to the time point, from 1 to T
k	Index to the scenario number, from 1 to K
N	Number of high-dimensional noises
K	Number of discrete scenario trees
S	Number of generated scenarios

Parameters

$P(*)$	Data probability distribution
$\delta_{\max}$	Maximum value of power fluctuation
$\delta_{\min}$	Minimum value of power fluctuation
$\overline{x}$	Mean value

Variables

x	Real sample value
z	Random noise value
x'	Generated sample value
c	Condition value
x_i	The i-th real sample value
t	Time point
t_0	Start time
t_e	End time
$X_T^{t_0}$	Actual power vector
$C_T^{t_0}$	Predicted power vector
$Z_T^{t_0}$	Random noise vector
$X_T'^{t_0}$	Generated sample vector
$\delta(t)$	Power fluctuation at time t
$\varepsilon(\tau)$	Forecast error at the $\tau-$th time point
$P_f(\tau)$	Forecast power at the $\tau-$th time point
$P_a(\tau)$	Actual power at the $\tau-$th time point
S^k	Scenario value
Q^k	Probability of scenario value

[13], while WGAN-GP incorporating gradient penalty has been proposed to enhance training stability [14]. Conditional GANs (CGANs) have been utilized for photovoltaic and wind power scenario generation by incorporating forecast information as conditioning variables [15,16]. A conditional-style GAN framework has been developed to capture both diurnal and seasonal variations in renewable outputs [17]. Furthermore, federated learning combined with least squares GAN has been introduced to model spatiotemporal characteristics [18], and cross-modal data fusion techniques have been explored to generate multimodal scenario data [19]. In addition, hybrid architectures integrating GANs with auxiliary models, such as Long Short-Term Memory networks (SeqGAN-LSTM) [20] and WGAN employing support vector classifiers (C-WGAN-svc) [17], have demonstrated promising performance. Nevertheless, these GAN-based approaches generally require abundant training data to achieve stable convergence and satisfactory generation quality.

In practical applications, however, the availability of renewable energy data is often limited. Due to data confidentiality, restricted access, or the scarcity of extreme weather samples, only small datasets may be available for training. Under such few-shot conditions, GAN-based models are prone to instability and mode collapse, which significantly deteriorate the quality and diversity of generated scenarios [21]. Although few-shot learning has been explored in related domains such as load forecasting [22] and investment decision-making [23], its application in renewable energy scenario generation remains relatively limited. Existing solutions to the few-shot problem typically include model fine-tuning [22], data augmentation [24], and transfer learning [25]. However, for renewable scenario generation under strict data constraints—particularly in privacy-sensitive or extreme weather settings—effective and reliable generative frameworks are still scarce. Recently, diffusion models have demonstrated advantages in scenario generation, especially in terms of pattern coverage and training stability [26]. However, they are computationally intensive and inherently biased toward large-sample settings, limiting their applicability in small-data scenarios [27]. Moreover, mainstream small-sample learning paradigms—such as transfer learning, *meta*-learning, and federated learning—are primarily designed for point forecasting rather than probabilistic scenario generation.

Compared with diffusion-based generators and few-shot prediction models, the proposed SK-CGAN focuses on integrating statistical prior knowledge into the adversarial generation framework. By embedding structured statistical information into the generative process, SK-CGAN aims to enable effective scenario generation under limited data conditions while maintaining computational efficiency. The model is lightweight and particularly suitable for applications involving limited yet privacy-sensitive historical data, such as extreme weather scenarios. To address the above challenges, this paper proposes a combined methodology of statistical knowledge and conditional generative adversarial networks (SK-CGAN). The proposed framework integrates a discrete probability model constructed from historical statistical knowledge of power fluctuations and forecast errors with a CGAN-based generative architecture. By introducing structured statistical priors into the conditional space of CGAN, the method compensates for the limitations of purely data-driven learning under few-shot conditions. The main contributions of this paper are summarized as follows:

1) An SK-CGAN architecture for few-shot day-ahead and intra-day scenario generation: The proposed framework consists of discrete scenario tree construction, CGAN training, and CGAN guidance via scenario trees. This structured pipeline enables the generation of diversified scenario curves with high coverage of real renewable power trajectories.
2) CGAN guided by statistically derived discrete scenario trees: A joint two-dimensional discrete probability model of power fluctuations and forecast errors is established based on historical statistical knowledge. Combined with renewable power forecasts, a set of scenario trees with associated occurrence probabilities is generated. These scenario trees are used as conditional inputs to the CGAN generator. Compared with conditioning solely on forecast power, the proposed guidance mechanism allows exploration of broader regions in the data space, enhances diversity, and mitigates insufficient variability caused by limited samples.
3) Systematic analysis of the impact of random noise in SK-CGAN: Random noise enhances model flexibility and generalization ability; however, excessive noise may interfere with generator learning and reduce scenario usability and accuracy. This paper systematically investigates the influence of noise amplitude on scenario generation performance. Results show that, compared with conventional CGAN, appropriately reducing noise amplitude within SK-CGAN improves coverage without increasing power interval width.

The remainder of this paper is organized as follows. Section II reviews the principles of GAN and CGAN and discusses challenges in few-shot renewable scenario generation. Section III introduces the proposed SK-CGAN methodology. Section IV presents case studies based on real datasets and evaluates model performance. Finally, Section V concludes

the paper.

A. Principle of GAN and CGAN

GAN is an unsupervised learning model [28] consisting of two independent neural networks: a generator (G) and a discriminator (D). The generator produces data samples resembling real data, while the discriminator differentiates between generated and real samples x. Through adversarial learning, G enhances the realism of its output. Besides, a random noise variable z drawn from a prior distribution (such as Gaussian distribution) is fed into the generator G to improve the fitting and generalization abilities. Both the generated sample and the real sample are then presented to the discriminator, typically a binary classifier, to differentiate between them. Consequently, the optimization objective function of GAN is

$$\min_G \max_D V(G,D) = E_{x\sim p(x)}[\log D(x)] + E_{z\sim p(z)}[\log(1 - D(G(z)))] \tag{1}$$

CGAN is a supervised learning model that enhances the GAN training process by incorporating condition information, thereby increasing its specificity. In the context of renewable energy scenarios, forecast data are treated as the condition value c, which is input into both the generator G and discriminator D. Consequently, in the CGAN generator, to improve their fitting and generalization abilities, random noise z and the conditional value c are formed together as the input to G, generating the output sample $x' = G(z|c)$. The discriminator assesses not only the disparity between the generated sample x' and the actual sample x, but also whether x' meets the condition c. Therefore, the training objective of CGAN can be framed as a min–max optimization problem concerning conditional values:

$$\min_G \max_D V(G,D) = E_{x\sim p(x)}[\log D(x|c)] + E_{x'\sim p(x')}[\log(1 - D(x'|c))] \tag{2}$$

CGAN allows for greater control over generated outcomes through conditioning variables, enabling the specification of desired sample types or scenario attributes. The conditional information accelerates the generator's learning of the data distribution and aids the discriminator in distinguishing between generated and real samples, thereby facilitating quicker model convergence.

B. Difficulties in Scenario Generation of CGAN with few Samples

The effectiveness of GAN (or CGAN)-based scenario generation strongly depends on the availability of sufficient training samples. Under few-shot conditions with limited data, GAN-based models may encounter the following challenges.

1) Overfitting: With insufficient samples, the GAN (CGAN) model may learn only a limited subset of the training data, causing the generated distribution $P(x')$ to deviate from the underlying true distribution $P(x')$. In addition, the generator may inadvertently capture noise present in the training set rather than the intrinsic data structure.
2) Insufficient diversity: The generator may extract certain representative features; however, it fails to capture the complete variability of real-world data, resulting in an incomplete or overly concentrated distribution of generated samples.
3) Training instability: Due to the adversarial nature of the objective functions, the generator and discriminator are inherently in competition. When training data are limited, the discriminator may become excessively dominant, thereby hindering the generator's capacity to learn effectively and update its parameters in a stable manner.

2. Proposed model

This section presents SK-CGAN method to generate accurate day-ahead or intraday scenarios with limited samples. A two-dimensional discrete probability model based on statistical knowledge is firstly introduced, followed by the structure of CGAN. Finally, SK-CGAN's mechanism is explained, which utilizes a conditional GAN guided by discrete scenario trees.

A. Discrete Probability Models Based on Historical Statistical Knowledge

1) Historical statistical knowledge: Renewable energy sources, such as wind power, display significant temporal fluctuations and forecast errors compared with traditional fossil fuels. Among them, temporal fluctuation refers to the variation in wind power output due to natural factors such as wind speed, air pressure, and humidity, causing differences in power between successive time periods.

Power fluctuation $\delta(t)$ and forecast error $\varepsilon(\tau)$ are defined as follows:

$$\delta(t) = P_a(t+1) - P_a(t) \tag{3}$$

$$\varepsilon(\tau) = \frac{P_f(\tau) - P_a(\tau)}{P_N} \tag{4}$$

Typically, the historical statistical knowledge about power fluctuation and forecast error is limited to a small amount of data, which is non-sensitive and unclassified, and can be accessible from public sources or electric power company.

2) Discrete probability distribution of power volatility, based on historical statistical knowledge: $\delta_{\max}$ and $\delta_{\min}$ separately denotes the maximum value and the minimum value of the power fluctuation in a certain study period. The power fluctuation range from the minimum to the maximum can be divided into N_W intervals according to dataset characteristics and the probability for each interval is based on its occurrence frequency of the historical power fluctuations in this interval. Therefore, $\delta_{\max}$, $\delta_{\min}$,N_W and the probability for each interval can organized as a set of historical statistical knowledge.

Here, we use a $(2*N_W)$ matrix G_W to represent the discrete probability distribution of power volatility. G_W is expressed as:

$$G_W = \begin{bmatrix} G_W(1,1),\ldots,G_W(1,w),\ldots,G_W(1,N_W) \\ G_W(2,1),\ldots,G_W(2,w),\ldots,G_W(1,N_W) \end{bmatrix}, 1 \leqslant w \leqslant N_W \tag{5}$$

$$G_W(1,w) = \delta_{w,mid} \tag{6}$$

$$G_W(2,w) = P_w^{\delta} \tag{7}$$

$$\delta^{Int} = \frac{\delta_{\max} - \delta_{\min}}{N_W} \tag{8}$$

$$\delta_{w,\min} = \delta_{\min} + \delta^{Int} * (w-1) \tag{9}$$

$$\delta_{w,\max} = \delta_{\min} + \delta^{Int} * w \tag{10}$$

$$\delta_{w,mid} = \frac{\delta_{w,\max} + \delta_{w,\min}}{2} \tag{11}$$

where, $G_W(1,w)$ means the representative value of the fluctuation interval w,$\delta_{w,mid}$ is the middle value of the fluctuation interval w which is taken as the representative value of the fluctuation interval w; $G_W(2,w)$ represents the historical occurrence probability in the corresponding fluctuation interval w,which can be represented as P_w^{δ};δ^{Int} is the width of each of the fluctuation intervals.

For power grid operators, statistical knowledge of volatility can be obtained through simple statistical work on historical data, here, P_w^{δ} can be calculated as:

$$P_w^{\delta} = N_{\delta}(w)/N_{\delta} \tag{12}$$

where, N_{δ} is the total statistical number of new energy fluctuations between the adjacent sampling points based on history data, $N_{\delta}(w)$ is the total number of new energy fluctuations which falls into the interval $[\delta_{w,\min}, \delta_{w,\max}]$.

3) Discrete probability distribution of prediction error based on historical statistical knowledge: The magnitude of the prediction error is typically time-dependent. Usually, as the forecast time window extends, additional influencing factors accumulate, leading to increased prediction error. The forecast errors at each prediction time point can be calculated based on historical data, which are another kind of historical statistical knowledge. For example, in the ultra-short-term prediction with a time span of 4 h and a granularity of 15 min, the forecast errors of 16 prediction time points can be calculated according to the previous equation based on the forecast power and the actual power of historical data.

Here, we use a (2^*N_E) matrix G_E to express the prediction error in the study time span. G_E is expressed as:

$$G_E = \begin{bmatrix} G_E(1,1), ..., G_E(1,\tau), ..., G_E(1,T) \\ G_E(2,1), ..., G_E(2,\tau), ..., G_E(2,T) \end{bmatrix}, 1 \leqslant \tau \leqslant T \tag{13}$$

$$G_E(1,\tau) = P_{\tau}^{f} \tag{14}$$

$$G_E(2,\tau) = P_{\tau}^{\varepsilon} \tag{15}$$

where, $G_E(1,\tau)$ means the power predicted value P_{τ}^{f} at the $\tau-$th prediction time point, $G_E(2,\tau)$ is the historical average forecast errors P_{τ}^{ε} at the $\tau-$th prediction time point from the historical statistical knowledge;T is the number of the prediction time points in the time span from t_0 to t_e.

Similarly, P_{τ}^{ε} can be calculated through simple statistical work on historical data, which can be as:

$$\varepsilon_{\tau}^{av} = \frac{\sum_{l=1}^{N_{\varepsilon}} (P_{\tau,l}^{f} - P_{\tau,l}^{a})}{N_{\varepsilon}} \tag{16}$$

$$P_{\tau}^{\varepsilon} = \varepsilon_{\tau}^{av} P_N \tag{17}$$

where,ε_t^{av} is the average forecast error at the $\tau-$th prediction time point, N_{ε} is the total sample number of the prediction error at the $\tau-$th prediction time point based on history data, $P_{\tau,l}^{f}, P_{\tau,l}^{a}$ are separately the prediction power and the actual power of the $l-$th sample at the $\tau-$th prediction point.

4) Joint probability distribution of two-dimensional discrete random variables:

Accounting for the statistical knowledge of volatility and forecast errors, a joint two-dimensional discrete probability model of errors and fluctuations is proposed. The joint distribution function of the new energy power at the $\tau-$th prediction time point can be expressed as:

$$\begin{aligned} &P_{w,\tau} = P\{X = x_w, Y = y_{\tau}\} \\ &w = 1, 2, \cdots, N_W; \tau = 1, 2, \cdots, T \end{aligned} \tag{18}$$

where, $x_w \in G_W(1,w)$,$y_{\tau} \in G_E(1,\tau)$. Subsequently, the joint probability distribution can be shown in Fig. 1. Due to the limitations of actual fluctuations and prediction errors, many of $P_{w,\tau}$ values are exactly zero.

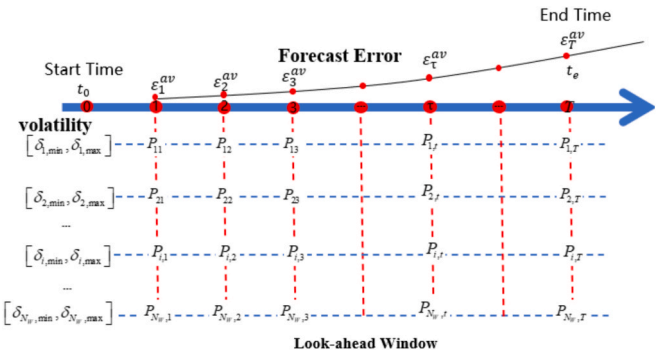

Fig. 1. Joint probability distribution of volatility and forecast errors.

B. Conditional Generative Adversarial Networks (CGAN).

The renewable power data at the $\tau-$th time point from the start time t_0, include the actual power value $P_{\tau}^{t_0,a}$ and the predicted value $P_{\tau}^{t_0,f}$, where T represents the total time span. For instance, in a four-hour prediction with 15-minute intervals, T equals 16.

Therefore, the actual power vector $X_T^{t_0}$ and predicted power vector $C_T^{t_0}$ can be combined into a sample at t_0 :

$$X_T^{t_0} = \{x_1, x_2, \cdots x_t \cdots, x_T\}, x_t = P_t^{t_0,a} \tag{19}$$

$$C_T^{t_0} = \{c_1, c_2, \cdots c_t \cdots, c_T\}, c_t = P_t^{t_0,f} \tag{20}$$

$$(X|C)_T^{t_0} = [(X_T^{t_0})^{\mathrm{T}}, (C_T^{t_0})^{\mathrm{T}}]^{\mathrm{T}} \tag{21}$$

To effectively capture the characteristics of renewable power, a convolutional neural network(CNN) is employed for both the generator and discriminator of CGAN. Unlike fully connected networks, CNNs excel at extracting local patterns in time series data, such as trends and periodic fluctuations via convolutional operations.

Inspired by the article [16], the random noise vector $Z_T^{t_0} = \{z_1, z_2, \cdots z_t \cdots, z_T\}$ from t_0 to $t_0 + T$ can be aligned in length with the predicted power vector $C_T^{t_0}$. These vectors are concatenated vertically into a matrix for input into the generator. The discriminator processes its input similarly, where the real sample vector $X_T^{t_0}$ are vertically concatenated with the predicted value vector $C_T^{t_0}$, and the generated sample vector $X_T'^{t_0} = \{x_1', x_2', \cdots x_t' \cdots, x_T'\}$ is formed by concatenating the predicted value sequence as input for the discriminator.

1) Generator: The proposed generator consists of two convolutional blocks, each comprising a convolution layer followed by an activation function. The first two convolution layers adopt two-dimensional convolutions with 3 × 3 kernels, combined with Batch Normalization and LeakyReLU activation functions. The 3 × 3 kernels effectively capture localized features and temporal patterns in renewable power sequences, including short-term trends and fluctuations. Batch Normalization facilitates training efficiency and promotes stable convergence, making it particularly suitable for time-series modeling tasks. The LeakyReLU activation function incorporates a negative slope, alleviating the "dead neuron" problem associated with standard ReLU, preserving responsiveness to negative inputs, and enhancing overall model robustness. The output layer of the generator employs the Tanh activation function to scale the generated values to the [–1, 1] interval, thereby stabilizing subsequent processing. Compared with ReLU, Tanh is symmetric and better accommodates negative-valued inputs, making it well suited for scenarios that require normalized outputs. The architectural structure of the generator is illustrated in Fig. 2.
2) Discriminator: The discriminator is designed for local feature extraction and differentiation between real and generated samples. It

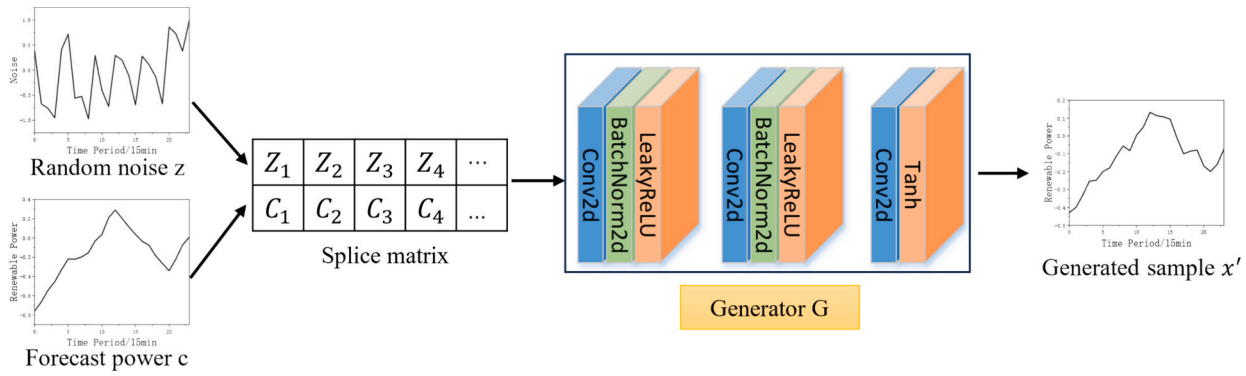

Fig. 2. Basic structure of generator.

consists of three convolution blocks followed by a fully connected layer. Each of the three convolution blocks comprises a two-dimensional convolution layer, Instance Normalization, and LeakyReLU activation functions. To classify the input values comprehensively, the high-dimensional data are flattened before passing through the fully connected layer, which outputs the discriminant value. The structure of the discriminator is depicted in Fig. 3.

Implementation details of conditioning: For each day-ahead horizon of length T, the generator receives three inputs: the forecast curve $\widehat{P} \in \mathbb{R}^T$, the scenario-tree features $s \in \mathbb{R}^{d_s}$, and a noise vector $z \in \mathbb{R}^{d_z}$. We first repeat and concatenate s and z along the temporal dimension so that all three components have compatible shapes, and then concatenate them along the feature dimension to obtain an input tensor of shape (T, d_{in}). This tensor is processed by a stack of fully connected or convolutional layers to produce a scenario trajectory in $\mathbb{R}^T$.

3) Loss function: During the training of traditional CGAN, the generator aims to enhance the discriminator output for the generated sample x', while the discriminator seeks to lower its output for x' and increase it for the real sample x. The respective loss functions of the generator and discriminator are defined as follows:

$$Loss_G = -E_{x' \sim p(x')}[D(x'|c)] \tag{22}$$

$$Loss_D = -E_{x \sim p(x)}[D(x|c)] + E_{x' \sim p(x')}[D(x'|c)] \tag{23}$$

The original GAN frequently faces training challenges and mode collapse, primarily due to the discriminator D employing JS divergence as its loss function. A significant disparity between generated and real samples can lead to vanishing gradients, complicating the training process. To mitigate this issue, this study integrates Wasserstein distance [29] into the discriminator's loss function to quantify the distance between the generated and real sample, defined as follows:

$$W(p(x), p(x')) = \inf_{\gamma \sim \Pi(p(x), p(x'))} E_{(x,x') \sim \gamma}[\|x - x'\|] \tag{24}$$

where γ denotes a joint distribution representing the optimal path, while $W(p(x), p(x'))$ represents the distance between distribution $p(x)$ and $p(x')$; $\Pi(p(x), p(x'))$ signifies the joint distribution of $p(x)$ and $p(x')$; $\|x - x'\|$ represents the distance between the real and generated samples. Since solving $\inf_{\Pi(p(x), p(x'))}$ is complex, the Kantorovich–Rubinstein dual form is commonly applied to describe the distance between generated and real samples in CGAN, expressed as:

$$W(p(x), p(x')) = \sup_{\|D(x)\|_L \leq K} E_{x \sim p(x)}[D(x|c)] - E_{x' \sim p(x')}[D(x'|c)] \tag{25}$$

where K_r denotes the constant of the Lipschitz function; $\|D(X)\|_L \leqslant K_r$ represents that the discriminator function satisfies the Lipschitz continuity condition of constant K_r.

Therefore, the final objective function of CGAN is as follows:

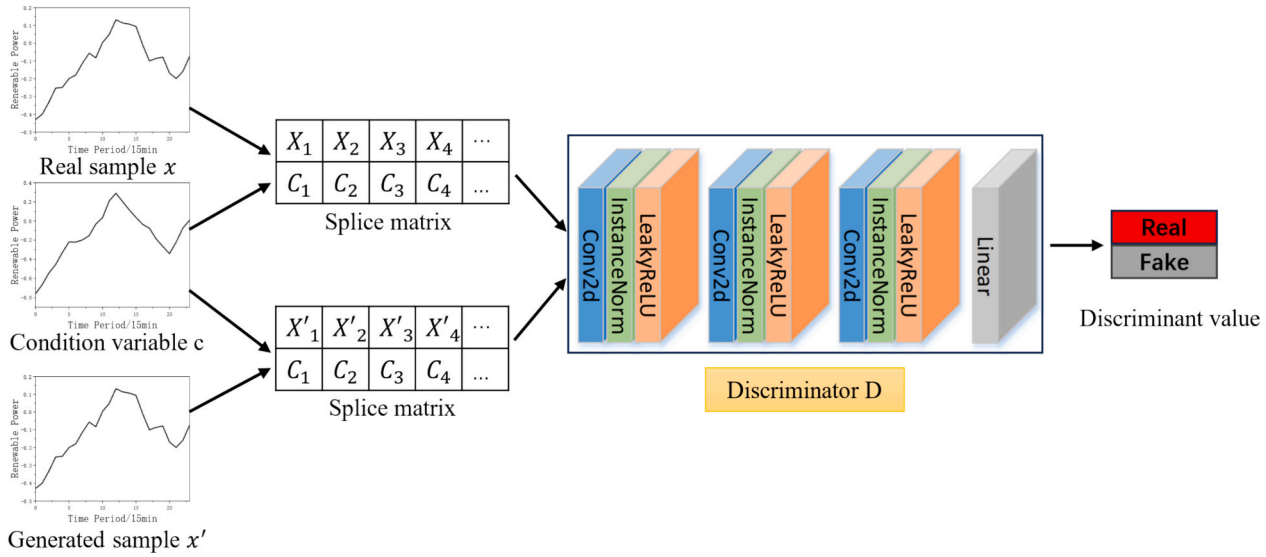

Fig. 3. Basic structure of discriminator.

$$\min_G \max_D V(G,D) = E_{x\sim p(x)}[\log D(x|c)] + E_{x'\sim p(x')}[\log(1-D(x'|c))] - \lambda E_{\hat{x}\sim p(\hat{x})}[\|\nabla D(\hat{x}|c)\|-1]^2 \quad (26)$$

where $\lambda E_{\hat{x}\sim p(\hat{x})}[\|\nabla D(\hat{x}|c)\|-1]^2$ denotes the gradient penalty term; $\hat{x}$ represents the real sample x and the generated sample x' are randomly sampled on the line.

C. Mechanism of SK-CGAN

The SK-CGAN architecture is illustrated in Fig. 4. The scenario generation of SK-CGAN includes the discrete scenario tree generation, the training of CGAN and CGAN guided by discrete scenario trees.

1) Training procedure of CGAN with few-shot learning: Firstly, the forecast data and few-shot historical data are normalized as the CGAN input set for training the networks of the generator G and the discriminator D. Training procedure of the networks of CGAN is shown in Fig. 5(1).
2) Discrete scenario trees based on historical statistical knowledge: Accounting for volatility and random errors, the joint probability distribution of errors and fluctuations is computed. After inputting renewable energy predictions into the discrete probability model, a set of scenario trees with occurrence probability is generated. Due to the large dimensionality, these trees are clustered into K classes using the k-means method, with the cluster center curves serving as typical discrete curves for the scenario trees. The set of typical curves can be listed as $\{S^1, S^2, ..., S^k, ..., S^K\}$, and their corresponding probabilities are $\{Q^1, Q^2, ..., Q^k, ..., Q^K\}$.
3) CGAN guided by discrete scenario trees: Discrete scenario trees based on statistical knowledge, which are separately input into the generator as the conditional values, can explore more diverse areas of the data space than the single predicted curve, yield a broader range of samples, and make up for the lack of diversity caused by small sample sizes. To avoid the increase of the power interval width of the generated scenario sets, we can appropriately reduce the amplitude range of random noises. Thus, a scenario curve S^k with probability Q^k from the discrete scenario tree is concatenated with N high-dimensional noises as input of the generator, which then outputs a set of scenarios. With K typical discrete scenario trees, this process will yield N^*K scenario sets for the forecast time windows. Scenario generation procedure guided by discrete scenario trees is shown in Fig. 5(2).

From a mechanistic standpoint, the proposed SK-CGAN can be interpreted as a CGAN framework regularized by a data-driven prior. The joint discrete probability model of volatility and forecast errors establishes a set of statistically plausible scenario trees, which are incorporated into the generator as additional conditional inputs. This design effectively enlarges the conditional space beyond the limited few-shot training trajectories, guiding the generator to learn within the intersection of historical statistical knowledge and available real samples, thereby alleviating overfitting and mitigating mode collapse. Meanwhile, the noise amplitude is deliberately calibrated to ensure that scenario diversity primarily originates from the structured discrete scenario trees rather than from unconstrained random perturbations.

3. Analysis of examples

This section outlines the datasets, experimental design, and analysis of renewable power scenario generation results. The performance of the proposed method is analyzed using various statistical indicators and compared with other scenario generation approaches. Taking both intra-day look-ahead and day-ahead as examples for scenario generation analysis and verification.

A. Evaluation Criteria

The following evaluation criteria are selected to assess the results of scenario generation[30]. The metrics for all tables are averages of the test samples.

1) Coverage rate (CR). The formula for the CR is:

$$CR = \frac{1}{T}\sum_{t=1}^{T} 1(x'_{t,\min} \leqslant x_t \leqslant x'_{t,\max}) \times 100\% \quad (27)$$

where $x'_{t,\min}$ is the minimum value of all generated samples at the time t; $x'_{t,\max}$ is the maximum value of all generated samples at the time t; x_t is the value of the real sample at time t. CR quantifies the percentage of actual renewable power values encompassed by the generated scenarios for the whole forecast time span. A higher CR signifies an increased likelihood that actual renewable power falls within the specified intervals, indicating an improved representation of renewable power variability.

2) 2)Power interval width (PIW). The formula for PIW is:

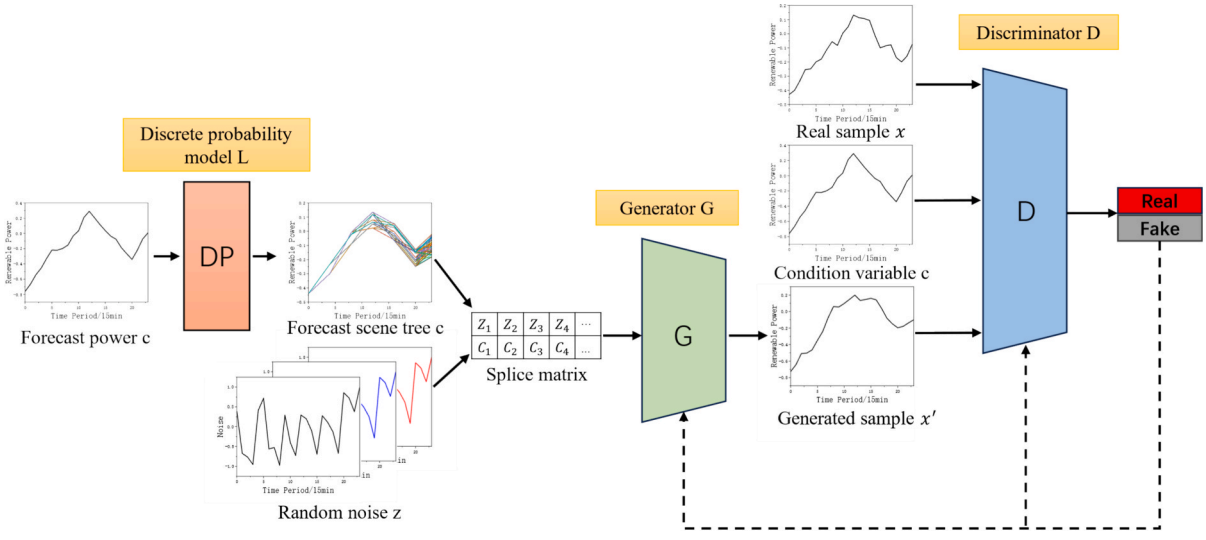

Fig. 4. Structure diagram of SK-CGAN.

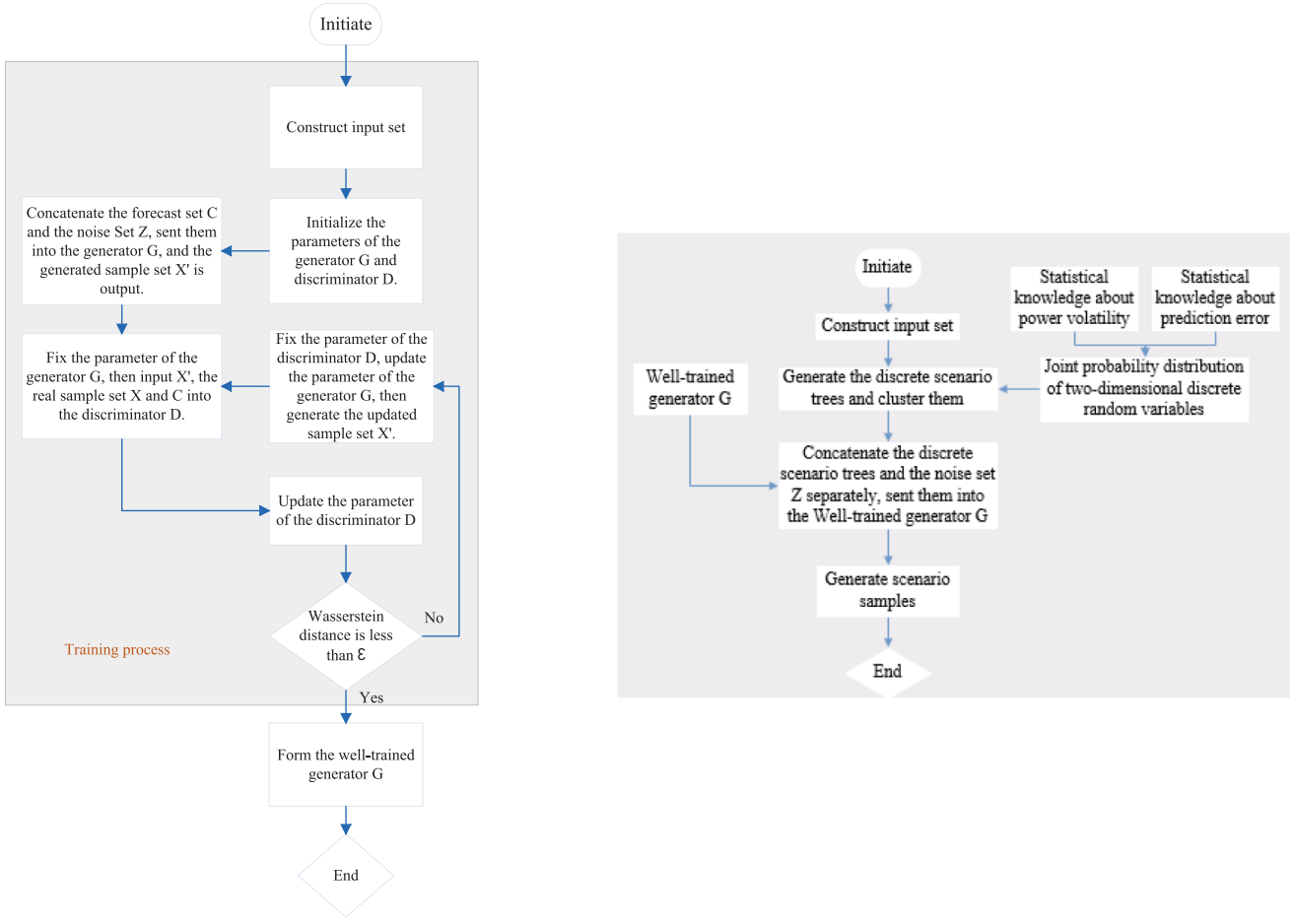

Fig. 5. Flow chart for SK-CGAN.

$$PIW = \frac{1}{T}\sum_{t=1}^{T}(x'_{t,\max} - x'_{t,\min}) \tag{28}$$

where CR denotes the coverage rate; PIW represents the average width of the power interval in the generated scenario set; $1(\bullet)$ is a binary variable that equals 1 if the condition in parentheses is met and 0 otherwise; T is the total number of time instances; x_t is the actual renewable power output at time t; $x'_{t,\min}$ and $x'_{t,\max}$ are the minimum and maximum values of all scenarios at time t, respectively. PIW denotes the average width of the power intervals within the renewable energy scenario set. This indicator evaluates the ability of the generated scenario to capture uncertainty. A smaller PIW indicates a closer consistency with the actual conditions, thereby characterizing the quality of the generated scenario set.

However, CR and PIW should not be used as independent evaluation criteria, they are typically employed as complementary indicators[31]. A larger CR combined with a smaller PIW offers a more accurate representation of renewable power uncertainty. Moreover, when CR values are comparable, a narrower PIW indicates greater model accuracy.

3) Energy score (ES): The formula for the ES is:

$$ES = \frac{1}{S}\sum_{s=1}^{s}\|x'_s - x\|_2 - \frac{1}{2\cdot S^2}\sum_{s=1}^{s}\sum_{s'=1}^{s}\|x'_s - x'_{s'}\|_2 \tag{29}$$

where S represents the number of generated scenarios; x' represents the renewable power output matrix for the $S-$th scenario; x represents the actual renewable power output matrix. The use of discretized scenarios in renewable power assessment illustrates the inherent uncertainty of these energy sources. The effective score (ES) serves as a key evaluation metric, where a lower ES value indicates a more accurate representation of the uncertainty in renewable power generation.

4) *Error analysis:* Mean absolute error (MAE) and root mean square error (RMSE) serve to assess the deviation between renewable power scenario values and actual values. The formulas for MAE and RMSE are as follows:

$$MAE = \frac{1}{s}\sum_{s=1}^{s}\frac{1}{T}\sum_{t=1}^{T}|x'_{s,t} - x_t| \tag{30}$$

$$RMSE = \sqrt{\frac{1}{S}\sum_{s=1}^{s}\frac{1}{T}\sum_{t=1}^{T}(x'_{s,t} - x_t)^2} \tag{31}$$

where $x'_{s,t}$ represents the scenario value at time t for the $S-$the scenario.

5) Autocorrelation coefficient: The generated scenarios must adhere to the temporal correlation inherent in renewable power outputs, as different time points exhibit a degree of correlation. To describe the distribution characteristics of renewable power output data over

time, the autocorrelation function (ACF) is commonly employed to represent this temporal correlation. The ACF is expressed as follows:

$$ACF_k = \frac{\sum_{t=1}^{T-k}(x_t - \bar{x})(x_{t+k} - \bar{x})}{\sum_{t=1}^{T}(x_t - \bar{x})^2} \tag{32}$$

where $\bar{x}$ represents the mean output of renewable power; k denotes the number of time intervals.

B. Experimental Design for intra-day look-ahead scenario generation

Due to limited availability, only 130 days of actual and ultra-short-term(4-hours look-ahead) forecast data of wind power and PV output can be obtained from a provincial grid in Northwest China, with 15-minute intervals[32].

The experiment consists of three parts for comparison: ①30 days of data were used for training, with 10 days from the remaining data used for validation; ②60 days were selected for training, followed by 10 days for validation; ③120 days were used for training, with the final 10 days for validation. The same validation set was used for the comparison between 3 parts.

The experiments were conducted using PyTorch on a computer with an NVIDIA RTX 3060 graphics card and an Intel Core i7-12700H (2.70 GHz).

Experiments were conducted using SK-CGAN and CGAN methods, following the three parts outlined in the previous experimental design. In this study, the ultra-short-term average forecast errors are provided by the power company which can be calculated based on historical data according to equation (21). As shown in Fig. 6, the prediction error of renewable energy often tends to increase with the time between the current point and the prediction point. Similarly, the actual power fluctuation range for the renewable energy of this area spans from –2200 to 2200 MW. To mitigate excessive dimensionality in the scenario tree generated by the discrete probability model, the volatility interval was segmented into the following ranges based on the historical volatility distribution: [–2200,–1500], [–1500,–1000], [–1000,–500], [–500,–250], [–250,0], [0, 250], [250, 500], [500, 1500], and [1500, 2200].

1) Scenario comparison: Targeting the climbing, peak, decline and trough period of renewable energy, SK-CGAN and CGAN methods are used to generate 100 scenarios for the ultra-short-term look-ahead time window in the same test set, respectively, as shown in Fig. 7. During the ramp-up period, due to the increased prediction errors, the scenario generated in Fig. 7(1b) cannot fully cover the actual renewable energy power curve, while the scenario set in Fig. 7 (1a) effectively covers the actual renewable power curve in the latter half. For the trough period, the scenario set in Fig. 7(4b) fails to completely cover the actual output curve, while the set in Fig. 7(4a) does so successfully. This comparison illustrates that SK-CGAN effectively captures the essential characteristics of renewable power by accounting for ultra-short-term forecast errors and historical volatility.
2) Time series analysis: The autocorrelation coefficient is used to assess the correlation within time series. Evaluating the time series correlation of generating scenarios is crucial for power system operation and scheduling, as it indicates the alignment of time characteristics in the scenarios with actual renewable energy data. Fig. 8 demonstrates that the autocorrelation coefficient curves of the actual data are effectively represented in the generated scenario, which nearly replicates the characteristics of the actual data.
3) Statistical metric comparison: To ensure rigorous validation, 100 scenarios or 200 scenarios are generated separately for each predicted curve in the validation set. The generated scenarios are evaluated using five statistical indicators: CR, PIW, ES, MAE, and RMSE. The averaged indicators of the validation set are as shown in Table 1. It can be seen:①As the training data grew from 10 days to 120 days, various indicators also improved.②SK-CGAN can significantly improve the CR indicator without increasing WID or slightly increasing it, especially in few-shot situations.③SK-CGAN improves the coverage of generating 100 scenarios, reduces the power interval width, and the ES, MAE, and RMSE of SK-CGAN are also much better than CGAN. However, for generated 200 scenarios, SK-CGAN improves the coverage rate, but increases the power interval width due to the dispersion of discrete scenario trees without changing the noise.

When using SK-CGAN, we can attempt to achieve WID invariance or WID reduction by reducing the noise amplitude, to improve CR. Table 2 gives the change of the evaluation indicators when the noise coefficient w_{nc} which means the ratio of the current noise to the original noise takes different values. We can see that with the decreasing of the noise, the indicators CR and WID are simultaneously decreasing. When$w_{nc} = 0.72$, the WID indicator using SK-CGAN is the same as when using CGAN, but the CR indicator has increased from 63.59% to 88.36%.

The Pairwise Distance (PD) metric is a commonly used measure for evaluating the diversity of generated samples. It is particularly prevalent in domains such as Generative Adversarial Networks (GANs), diffusion models, and probabilistic forecasting, where assessing the degree of variation among generated outputs is critical. This metric is especially effective in identifying issues such as mode collapse or over-concentration of generated results[33].

The core idea of Pairwise Distance is to compute the distance between every pair of generated samples within a given set and then

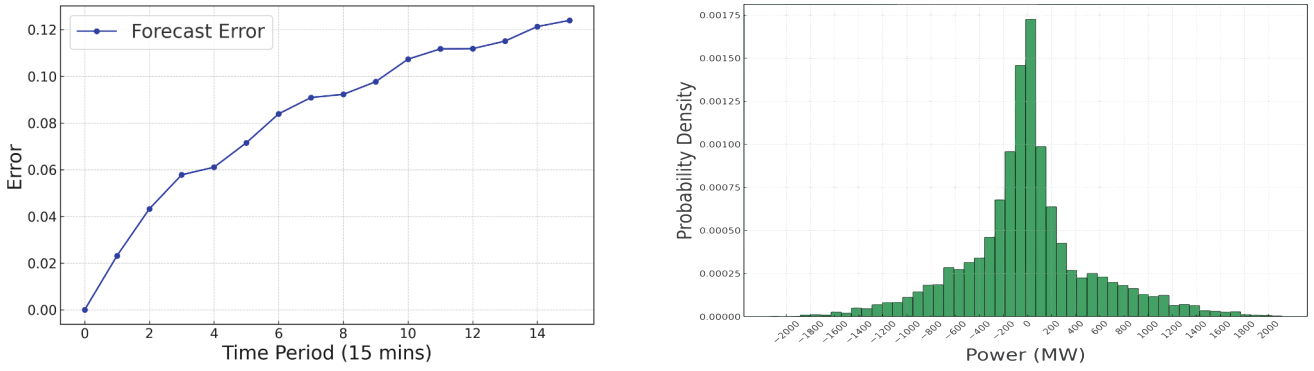

(1) Historical mean error of ultra-short-term forecast **(2)** Probability distribution of historical fluctuations

Fig. 6. Historical Statistical Knowledge.

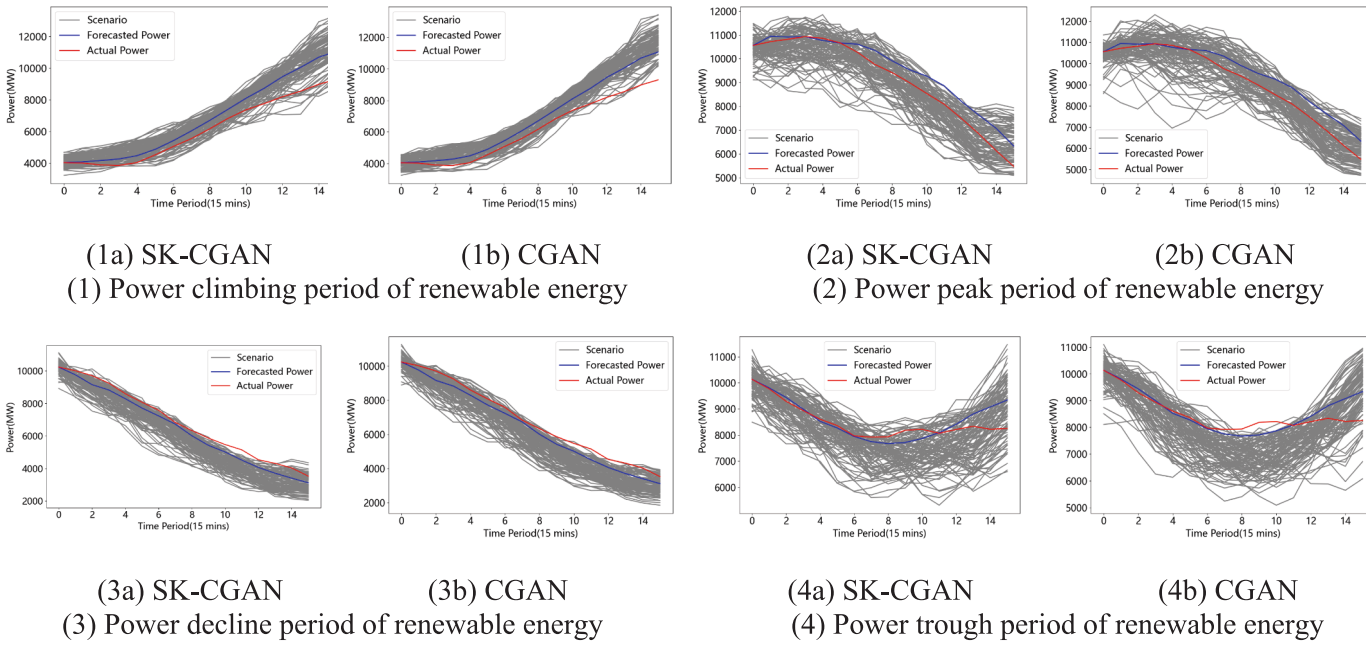

Fig. 7. Scenario result comparison of the SK-CGAN and CGAN methods.

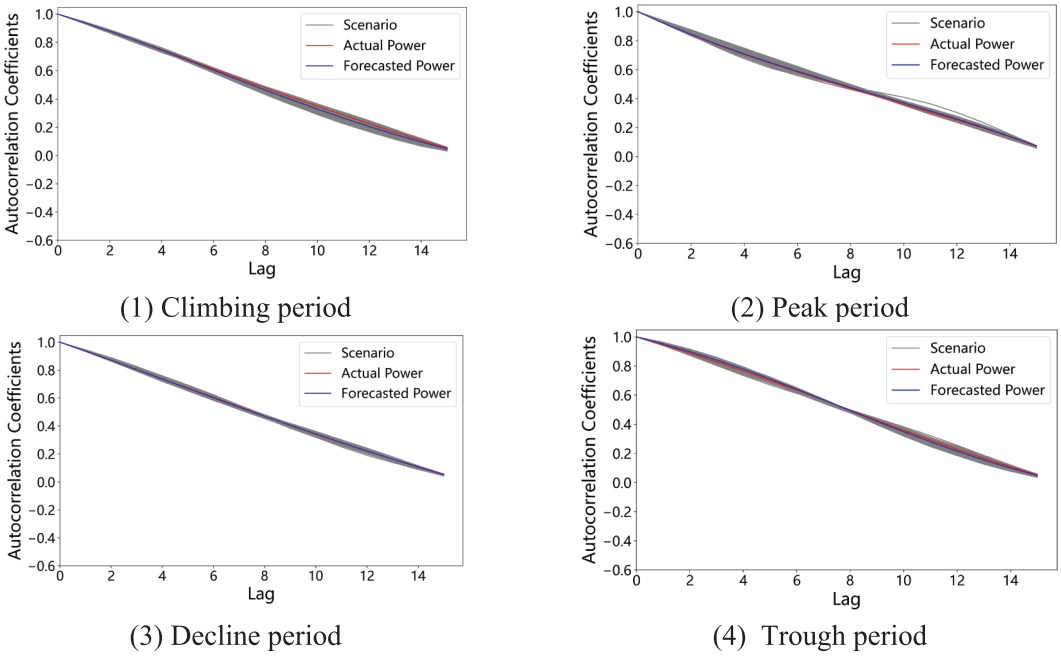

Fig. 8. Autocorrelation coefficient of SK-CGAN method for 4 typical intra-day scenarios.

summarize these distances—typically through their mean or statistical distribution. It reflects how different the generated samples are from one another. A generally low PD value suggests that the samples are highly similar, potentially indicating insufficient diversity or mode collapse. Conversely, a higher PD value implies greater variation among the samples, which corresponds to stronger diversity in the generative model's output.

Formally, the PD metric quantifies diversity by calculating pairwise distances across all generated samples in a set $\{x_i\}$, and is defined as:

$$D = \frac{2}{N(N-1)} \sum_{i<j} d(x_i, x_j) \tag{33}$$

PCA-Variance Diversity (PCA-VD) is a metric used to evaluate the diversity among generated scenarios. It treats the set of generated samples—such as multiple time series, images, or trajectories—as high-dimensional data and projects them into a lower-dimensional space using Principal Component Analysis (PCA). The diversity is then quantified based on thevariance contributions of the principal components.

Typically, the value of this metric falls within the following ranges:

- 0.2–0.6: indicates *low diversity*, where most variance is captured by only a few components;
- 0.6–0.9: represents *moderate diversity*;

Table 1
Evaluation metrics results.

	Method	Sample days	CR	PIW	ES	MAE	RMSE		Method	Sample days	CR	PIW	ES	MAE	RMSE
100 generated scenarios	WGAN	10	58.6%	1.34	1.03	0.38	0.43	200 generated scenarios	WGAN	10	77.5%	1.18	0.66	0.27	0.31
	CGAN		59.6%	0.15	0.26	0.075	0.087		CGAN		72.3%	**0.25**	0.27	0.085	0.097
	SK-CGAN		**68.3%**	**0.28**	**0.37**	**0.12**	**0.13**		**SK-CGAN**		**79.3%**	**0.20**	**0.22**	**0.066**	**0.078**
	WGAN	30	81.4%	1.21	1.25	0.45	0.49		WGAN	30	92.1%	1.44	0.86	0.36	0.41
	CGAN		74.1%	0.34	0.32	0.11	0.13		CGAN		72.3%	**0.25**	0.27	0.085	0.097
	SK-CGAN		**84.8%**	**0.28**	**0.25**	**0.087**	**0.10**		SK-CGAN		**93.1%**	0.26	**0.20**	**0.069**	**0.081**
	WGAN	60	87.3%	1.37	1.20	0.44	0.48		WGAN	60	86.3%	1.52	0.91	0.37	0.42
	CGAN		80.7%	0.34	0.30	0.10	0.12		CGAN		79.8%	**0.22**	0.21	0.068	0.0793
	SK-CGAN		**88.3%**	**0.33**	**0.25**	**0.09**	**0.11**		**SK-CGAN**		**93.9%**	**0.28**	**0.17**	**0.06**	**0.0713**
	WGAN	120	86.2%	1.34	0.95	0.37	0.42		WGAN	120	91.1%	1.45	0.92	0.37	0.4131
	CGAN		96.1%	0.30	0.17	0.068	0.082		CGAN		96.7%	**0.31**	0.17	0.067	0.0801
	SK-CGAN		**96.2%**	**0.30**	**0.16**	**0.066**	**0.08**		**SK-CGAN**		**97.3%**	**0.33**	**0.17**	**0.066**	**0.0787**

TABLE 2
Evaluation metrics results.

Indices	CGAN	SK-CGAN					
		$w_{nc} = 1.00$	$w_{nc} = 0.95$	$w_{nc} = 0.80$	$w_{nc} = \mathbf{0.72}$	$w_{nc} = 0.67$	$w_{nc} = 0.50$
PIW	**0.2150**	0.2430	0.23827	0.2263	**0.2150**	0.2092	0.1907
CR	**63.59%**	93.45%	92.59%	90.57%	**88.36%**	87.33%	83.64%
MAE	**0.0915**	0.0663	0.0670	0.069	**0.0713**	0.0724	0.0761
RMSE	**0.1030**	0.0782	0.0789	0.0812	**0.0838**	0.0851	0.0896
ES	**0.3123**	0.1696	0.1993	0.2131	**0.2279**	0.2358	0.2616

- >0.9: reflects *high diversity*, with multiple principal components contributing substantially.

The PCD-VD metric is calculated by performing PCA on the generated scenario matrix and summing the variance contributions of the top K principal components as follows:

$$D_{PCA-VD} = \sum_{k=1}^{K} \frac{\lambda_k}{\sum_i \lambda_i} \tag{34}$$

When the generated results exhibit strong diversity, multiple samples are more widely dispersed in the high-dimensional space, and several principal components contribute with relatively high variance, resulting in a larger PCD-VD value. Conversely, if the generated results are overly concentrated or suffer from mode collapse, the variance becomes dominated by only a few principal components, leading to a lower value.

Therefore, the PCA-Variance Diversity metric provides an effective measure for evaluating the sample diversity of generative models.

As shown in Table 3, SK-CGAN demonstrates significant superiority over CGAN across all time horizons. Both the Pairwise Distance (PD) and PCA-Variance Diversity (PCA-VD) metrics indicate that SK-CGAN generates richer, more divergent, and structurally diverse scenario sets, effectively mitigating the mode collapse problem commonly observed in traditional CGANs.

In short-term forecasts (30-day and 60-day horizons), CGAN exhibits a clear lack of diversity, whereas SK-CGAN consistently maintains a high diversity level close to 0.9. For the 120-day prediction, both models display relatively high PCA-VD values, which can be attributed to the accumulation of long-term prediction errors that naturally lead to scenario divergence. Nevertheless, the PD and PCA-VD of SK-CGAN remain stable, suggesting that its diversity stems from well-structured multimodal generation rather than from unconstrained random drift, as appears to be the case for CGAN.

TABLE 3
Evaluation metrics results.

Noise distribution type	Sample days	PD	PCA-VD
CGAN	30	0.2163	0.2362
SK-CGAN		0.9319	0.9384
CGAN	60	0.1565	0.2103
SK-CGAN		0.8816	0.9066
CGAN	120	0.2764	0.9592
SK-CGAN		0.2894	0.9601

As shown in Fig. 9, a larger CR value indicates better performance, while a smaller PIW value is preferred. Both metrics improve as the number of samples increases. However, compared with CGAN, SK-CGAN exhibits consistently better performance within the 10-day and 30-day intervals. By the 120-day horizon, the performance gap between the two models narrows, yet SK-CGAN still maintains a slight advantage.

As illustrated in Fig. 10, when the training sample size is limited, CGAN performs noticeably worse than SK-CGAN. This can be attributed to the relatively large number of parameters in CGAN and its high variance characteristics, which make the discriminator prone to becoming overly dominant. Such imbalance often leads to unstable generator training or even mode collapse. In contrast, SK-CGAN incorporates statistical knowledge to restrict the data space to *a historically and statistically plausible region*, effectively increasing model bias while reducing variance, thereby enhancing generalization performance.

As the number of training samples increases, the relative contribution of the statistical knowledge constraint gradually decreases. Under sufficient data support, CGAN is capable of learning the data distribution more effectively, and the performance improvement achieved by SK-CGAN is primarily due to its refined prior representation of forecast errors. Consequently, the overall performance gap between the two models narrows. Furthermore, as shown in Tables 2 and 4, for a fixed training dataset, adjusting the noise amplitude and distribution enables a controllable trade-off among different evaluation metrics. This observation indicates that, even with fixed data availability, the intensity of prior constraints and the diversity introduced by noise significantly influence scenario quality, thereby providing further insight into the interplay between data sufficiency and model performance.

As shown in Table 4, the impact of different noise distribution types on scenario generation is further examined. The experimental results indicate that both Laplace and Gaussian noise distributions substantially improve the performance of the SK-CGAN model, demonstrating strong adaptability and generalization capability. Specifically, Laplace noise outperforms all other distributions across multiple evaluation metrics,

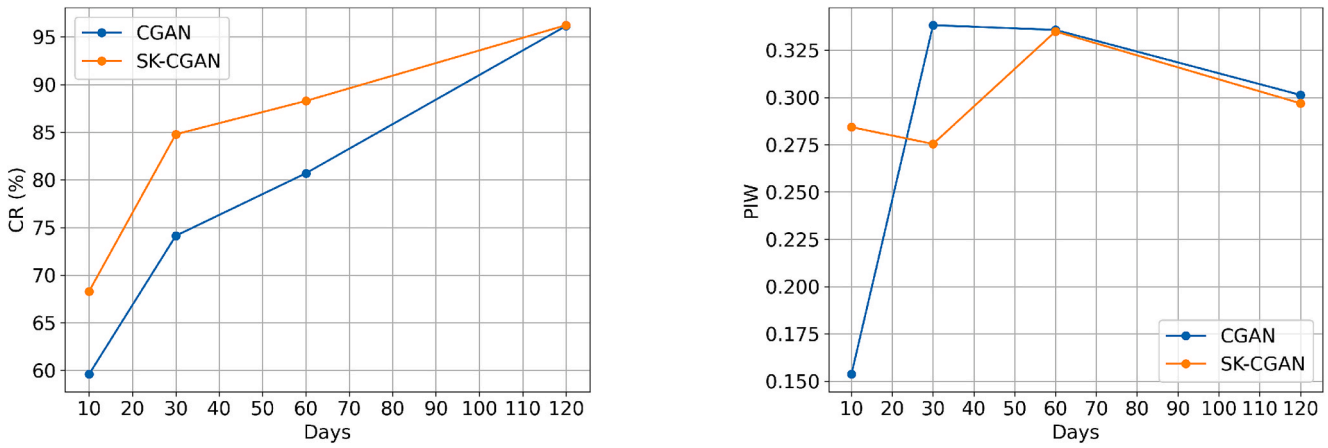

Fig. 9. The line comparison chart of CR and PIW indicators of CGAN and SK-CGAN.

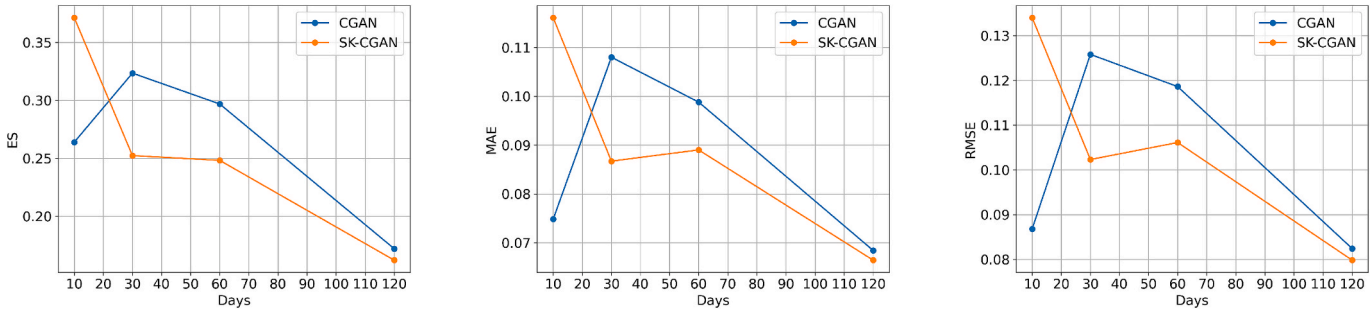

Fig. 10. The line comparison chart of ES, MAE and RMSE indicators of CGAN and SK-CGAN.

TABLE 4
Evaluation metrics results.

Noise distribution type	CR	PIW	ES	MAE	RMSE
Gaussian	89.59%	0.2014	0.1881	0.0644	0.0762
Uniform	83.58%	0.1868	0.2334	0.0729	0.0860
Laplace	98.41%	0.3100	0.1498	0.0637	0.0760
Poisson	89.82%	0.2470	0.2238	0.0707	0.0900

achieving the highest CR of 98.41% and the lowest MAE and RMSE values of 0.0637 and 0.0760, respectively. In addition, it yields the lowest ES (0.1498), indicating superior quality of the predicted intervals. Although its PIW is relatively larger, this can be interpreted as a reasonable trade-off to guarantee high coverage reliability. In contrast, Gaussian noise exhibits balanced and stable performance across all metrics, with a CR of 89.59%, MAE of 0.0644, RMSE of 0.0762, and a relatively low ES of 0.1881, all of which are comparable to those achieved under Laplace noise. Overall, Laplace noise is more appropriate for applications requiring high generation accuracy and interval reliability, whereas Gaussian noise provides a better balance between precision and stability, making it highly practical for real-world deployment.

In practical implementation, a validation-based strategy is adopted to determine the noise configuration. A predefined set of candidate noise amplitudes and distribution types is first established. For each candidate configuration, the model is trained and evaluated on a validation subset using the CR, PIW, and ES metrics. The final noise configuration is selected as the one that achieves the target nominal coverage while maintaining a reasonably narrow interval width and a satisfactory ES value. Once determined, the resulting scenario bands can be interpreted as empirical confidence intervals centered around the day-ahead forecast.

C. Experimental Design for day-ahead scenario generation of extreme weather.

In this case study, the actual power outputs of renewable energy sources, together with the corresponding day-ahead short-term forecasts at hourly resolution, were obtained from a provincial-level power grid in Northwest China under extreme cold-wave conditions. A total of 27 days of extreme weather data were collected, of which 20 days were used for training and the remaining 7 days for testing. The statistical knowledge—namely, the average forecast errors and fluctuation distributions illustrated in Fig. 12—was derived exclusively from the training set. During the testing phase, for each of the seven unseen days, only the day-ahead forecast curve was provided as the conditional input to the generator, while the corresponding actual power outputs were reserved solely for out-of-sample evaluation.

Fig. 11 illustrates two key statistical characteristics that serve as essential prior knowledge for model development: historical forecast errors under extreme weather and the probability distribution of hourly power fluctuations. As shown in Fig. 11(1), the average forecast error across different hours increases significantly during daytime periods, particularly between 08:00 and 16:00. This indicates that renewable power output exhibits pronounced volatility and heightened forecasting uncertainty during these hours, thereby posing substantial challenges to accurate modeling. Fig. 11(2) presents the distribution of historical fluctuation magnitudes, showing that most variations lie within ± 150 MW. Nevertheless, a noticeable frequency of extreme fluctuation events exceeding ± 400 MW is observed, highlighting the heavy-tailed behavior and abrupt variability of renewable power output under extreme weather conditions.

As illustrated in Fig. 12, the generation performance of SK-CGAN and CGAN is evaluated across four representative extreme weather samples. The results indicate that although CGAN shows partial capability in

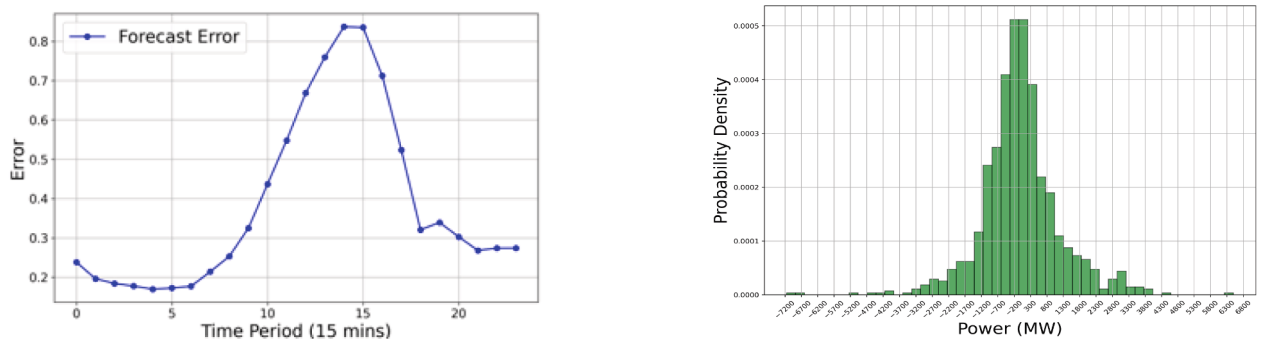

(1) Average error of day-ahead short-term forecasts (2) Hourly-level historical fluctuation probability distribution

Fig. 11. Statistical Knowledge of Historical Data Under Extreme Scenarios.

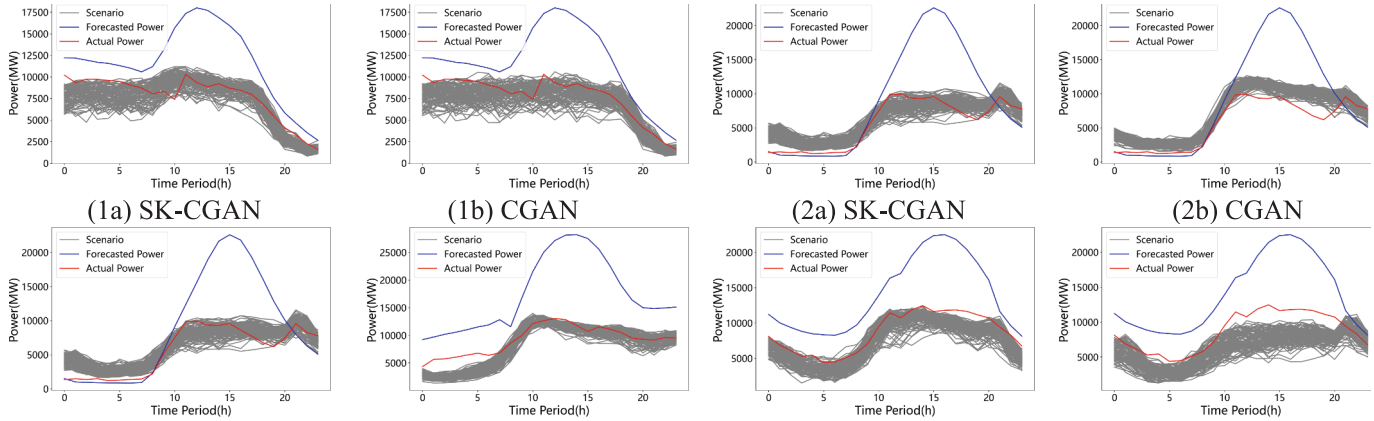

(1a) SK-CGAN (1b) CGAN (2a) SK-CGAN (2b) CGAN

(3a) SK-CGAN (3b) CGAN (4a) SK-CGAN (4b) CGAN

Fig. 12. Extreme Scenarios Generated by SK-CGAN and CGAN.

capturing structural characteristics, its generated scenarios exhibit significant contraction in regions with abrupt fluctuations. This contraction leads to noticeable discrepancies between the scenario boundaries and actual values, thereby limiting its ability to accurately represent extreme trends and rapid transitions. In contrast, SK-CGAN demonstrates substantially improved performance in both boundary coverage and trend reconstruction across diverse extreme scenarios. During critical periods—such as sudden power surges, quasi-steady phases, and sharp post-peak declines—the generated scenarios from SK-CGAN consistently align with the upper and lower envelopes of the actual trajectories. Furthermore, the generated scenarios exhibit balanced dispersion and enhanced diversity, reflecting the model's strengthened capability in capturing localized structural variations. These results highlight the robustness of SK-CGAN in modeling the complex and highly volatile dynamics characteristic of extreme weather conditions.

TABLE 5. provides a comparative evaluation of different models on the 7-day test set. The results demonstrate that SK-CGAN achieves the best performance across all five evaluation metrics. Specifically, the Coverage Rate (CR) of SK-CGAN reaches 0.6905, representing a 10.12% improvement over CGAN and indicating significantly enhanced capability in enveloping extreme power outputs. The Prediction Interval Width (PIW) is 0.2294, lower than that of CGAN, suggesting that the model effectively compresses the fluctuation bandwidth while preserving adequate coverage. The ES for SK-CGAN is 0.3672, substantially better than CGAN's 0.4497, reflecting improved capability in capturing the probabilistic structure of power output distributions. In terms of point forecasting accuracy, SK-CGAN achieves a Mean Absolute Error (MAE) of 0.0919 and a Root Mean Square Error (RMSE) of 0.1107, corresponding to reductions of 10.8% and 11.3%, respectively, compared with CGAN. These improvements demonstrate enhanced precision in point-wise prediction. Overall, the SK-CGAN model exhibits stronger capability in modeling local disturbances, representing output boundaries, and maintaining structural consistency under extreme weather conditions. Consequently, it generates power scenarios that are both physically plausible and statistically reliable, thereby providing robust data support for power system scheduling and optimization in extreme scenarios.

TABLE 5
Autocorrelation coefficient curve of extreme scenarios generated by SK-CGAN.

Method	CR	PIW	ES	MAE	RMSE
CGAN	58.93%	0.2472	0.4497	0.1037	0.1248
SK-CGAN	**69.05%**	**0.2294**	**0.3672**	**0.0919**	**0.1107**

4. Conclusion

To address the challenges of few-shot renewable scenario generation caused by data confidentiality and limited historical records, this paper proposes an SK-CGAN architecture that integrates statistical knowledge of historical fluctuations and wind power forecast errors with conditional generative adversarial networks. Simulation results verify the feasibility and effectiveness of the proposed method. Compared with conventional CGAN, SK-CGAN improves the coverage rate of generated scenarios without increasing the power interval width, thereby achieving more reliable uncertainty representation under small-sample conditions. The proposed framework can be extended to other small-sample scenario generation tasks, such as extreme weather and demand response scenarios. Future work will focus on adaptive noise

configuration and further validation of statistical knowledge effectiveness.

CRediT authorship contribution statement

Ke Wang: Writing – review & editing, Writing – original draft, Project administration, Methodology, Funding acquisition, Data curation, Conceptualization. **Yinan Zhou:** Writing – original draft. **Yuanxing Xia:** Methodology. **Jun Liang:** Writing – review & editing. **Xiangkuan Wan:** Conceptualization.

Funding

This work was supported by National Natural Science Foundation of China (No. 52377092); Fundamental Research Funds for the Central Universities (B240201053) and Natural Science Foundation of Anhui Province (JZ2022AKZR0725).

Declaration of competing interest

The authors declare that they have no known competing financial interests or personal relationships that could have appeared to influence the work reported in this paper.

Data availability

The authors do not have permission to share data.

References

[1] M. Hutchinson and F. Zhao, "GWEC global wind report 2023," *Global Wind Energy Council,* Mar 2023. [Online]. Available: https://gwec.net/globalwindreport2023/.
[2] Francois B, Borga M, Creutin JD, Hingray B, Raynaud D, Sauterleute JF. Complementarity between solar and hydro power: sensitivity study to climate characteristics in Northern-Italy. Renew Energy Feb. 2016;86:543–53.
[3] L. Bird, Debra.L, Michael R. M, Enrico M.C, Ana , Damian F *et al.*, "Wind and solar energy curtailment: A review of international experience," *Renew. Sustain. Energy Rev.*, vol. 65, pp. 577–586, Nov. 2016, doi: 10.1016/j.rser.2016.06.082.
[4] Xue YS, Lei X, Xue F, Yu C, Dong ZY, Wen FS, et al. A review on impacts of wind power uncertainties on power systems. Proc CSEE 2014;34(29):5029–40.
[5] Yan J, Zhang Y, Liu C, Han S, Li L, Liu G, et al. Reviews on uncertainty analysis of wind power forecasting. Renew Sustain Energy Rev Dec. 2015;52:1322–30.
[6] Sun Y, Zhong J, Li Z, Tian W, Shahidehpour M. Stochastic scheduling of battery-based energy storage transportation system with the penetration of wind power. IEEE Trans Sustain Energy Jan. 2017;8(1):135–44.
[7] Wu H, Shahidehpour M, Alabdulwahab A, Abusorrah A. Demand response exchange in the stochastic day-ahead scheduling with variable renewable generation. IEEE Trans Sustain Energy Apr. 2015;6(2):516–25.
[8] Hart EK, Jacobson MZ. A Monte Carlo approach to generator portfolio planning and carbon emissions assessments of systems with large penetrations of variable renewables. Renew Energy Aug. 2011;36(8):2278–86.
[9] Cheng J, Gicquel C, Lisser A. Partial sample average approximation method for chance constrained problems. Optim Lett Feb. 2019;13(4):657–72.
[10] Chen Y, Wen J, Cheng S. Probabilistic load flow method based on Nataf transformation and Latin hypercube sampling. IEEE Trans Sustain Energy Apr. 2013;4(2):294–301.
[11] Qiu Y, Li Q, Pan Y, Yang H, Chen W. A scenario generation method based on the mixture vine copula and its application in the power system with wind/hydrogen production. Int J Hydrogen Energy Feb. 2019;44(11):5162–70.
[12] Y. Qi, W. Hu, Y. Dong, Y. Fan, L. Dong, and M. Xiao, "Optimal con-figuration of concentrating solar power in multienergy power systems with an improved variational autoencoder," *Applied Energy,* vol. 274, Sep. 2020, Art. no. 115124.
[13] Chen Y, Wang Y, Kirschen D, Zhang B. Model-free renewable scenario generation using generative adversarial networks. IEEE Trans Power Syst May 2018;33(3):3265–75.
[14] Zhang Y, Ai Q, Xiao F, Hao R, Lu T. Typical wind power scenario generation for multiple wind farms using conditional improved Wasserstein generative adversarial network. Int J Electr Power Energy Syst Jan. 2020;114:105388. https://doi.org/10.1016/j.ijepes.2019.105388.
[15] Yang X, He H, Li J, Zhang Y. Toward optimal risk-averse configuration for HESS with CGANs-based PV scenario generation. IEEE Trans Syst Man Cybern Mar. 2021;51(3):1779–93.
[16] X. Dong, Y. Sun, and T. Pu, "Day-ahead scenario generation of renewable energy based on conditional GAN," *Proceedings of the CSEE,* vol. 40, no. 17, pp. 5527–5536, Sep. 2020. (in Chinese). doi: 10.13334/j.0258-8013.pcsee.190633.
[17] Yuan R, Wang B, Sun Y, Song X, Watada J. Conditional style-based generative adversarial networks for renewable scenario generation. IEEE Trans Power Syst Mar. 2023;38(2):1281–96.
[18] Li Y, Li J, Wang Y. Privacy-preserving spatiotemporal scenario generation of renewable energies: a federated deep generative learning approach. IEEE Trans Ind Inform Apr. 2022;18(4):2310–20.
[19] Kang MY, Zhu R, Chen DX, Li CJ, Gu W, Qian XS, et al. A cross-modal generative adversarial network for scenarios generation of renewable energy. IEEE Trans Power Syst, Mar 2024;39(2):2630–40.
[20] Liang J, Tang W. Sequence generative adversarial networks for wind power scenario generation. IEEE J Sel Areas Commun Jan. 2020;38(1):110–8.
[21] J. Lan, Y. Zhou, Q. Guo, and H. Sun, "Data augmentation for data-driven methods in power system operation: a novel framework using improved gan and transfer learning," *IEEE Trans. Power Syst.,* 39[2025-01-16]. DOI:10.1109/TPWRS.2024.3364166.
[22] X. SUN, J. LI, and B. ZENG, "Small-sample day-ahead power load forecasting of integrated energy system based on feature transfer learning," *Control Theory Applications,* vol. 38, no. 1, pp. 63 – 72, Jan. 2021. (in Chinese). doi: 10.7641/CTA.2020.00280.
[23] J. Yang, Y. Xiang Y, and Y. Liu, "Adaptive transfer learning of small sample correlation rules for distribution network investment decision," *Proceedings of the CSEE,* vol.40, no.17, pp.5823-5834, Aug. 2021. (in Chinese). doi: 10.13334/j.0258-8013.pcsee.210734.A. Nakamura and T. Harada, "Revisiting fine-tuning for few-shot learning," arXiv, preprint arXiv:1910.00216, Oct. 2019. doi: 10.48550/arXiv.1910.00216.
[24] Royle JA, Dorazio RM, Link WA. Analysis of multinomial models with unknown index using data augmentation. J Comput Graph Stat Mar. 2007;16(1):67–85.
[25] Y. Jang, H. Lee, S. J. Hwang, and J. Shin, "Learning What and Where to Transfer," in *Proceedings of the 36th International Conference on Machine Learning,* PMLR, May 2019, pp. 3030–3039.
[26] Xiao X, Wu Q, Jin X, Chen Y, Chang X, Liu Z, et al. Conditional denoising diffusion probabilistic model based ante-hoc explainable scenario generation for power systems dispatch. Electr Pow Syst Res Mar. 2025;238:110993. https://doi.org/10.1016/j.epsr.2025.110993.
[27] Dong X, Sun Y, Yang Y, Mao Z. Controllable renewable energy scenario generation based on pattern-guided diffusion models. Appl Energy Nov. 2025;398:126446. https://doi.org/10.1016/j.apenergy.2025.126446.
[28] I. J. Goodfellow, J. Pouget-Abadie, M. Mirza, B. Xu, D. Warde-Farley, S. Ozair *et al.,* "Generative adversarial nets," in *Proc. Adv. Neural Inf. Process. Syst.,* 2014, pp. 2672–2680.
[29] M. Arjovsky, S. Chintala, and L. Bottou, "Wasserstein generative adversarial networks," in *Proc. Int. Conf. Mach. Learn.,* 2017, pp. 214–223.
[30] X. Wang, Z. Hu, M. Zhang, and M. Hu, "Research on Establishment of Quality Evaluation Framework of Short-Term Wind Power Scenarios," *Power Syst Technol,* vol. 41, no. 5, pp. 1583-1589, May.2017.(in Chinese). doi: 10.13335/j.1000-3673.pst.2016.1985.
[31] Pinson P, Girard R. Evaluating the quality of scenarios of short-term wind power generation. Appl Energy Aug. 2012;96:12–20.
[32] Prósper MA, Otero-Casal C, Fernández FC, Miguez-Macho G. Wind power forecasting for a real onshore wind farm on complex terrain using WRF high resolution simulations. Renew Energy May 2019;135:674–86.
[33] Gao YJ, Xue FS, Yang WH, Yang Q, Sun YJ, Sun YP, et al. Optimal operation modes of photovoltaic-battery energy storage system based power plants considering typical scenarios. Prot Control Mod Power Syst Dec. 2017;2(1):36.

Ke Wang(Member, IEEE) received the M.S. degree in electrical engineering from State Grid Electric Power Research Institute, Nanjing, China, in 2004 and the Ph.D. degree in electrical engineering with China Electric Power Research Institute(CEPRI), Beijing, China, in 2018. From 2012 to 2022, she was a Senior Engineer with CEPRI. She is currently a Professor in College of Energy and Electrical Engineering, Hohai University, Nanjing, China. Her research interests mainly include flexible resource scheduling and the AI application in power system decision-making.

YinanZhou received the Bachelor's degree in Mechatronics from Nanjing Institute of Technology in 2019. He is currently pursuing a Master's degree in Electrical Engineering at Hohai University. His research interests include renewable energy scenario generation and the application of artificial intelligence in power systems.

Yuanxing Xia(Member, IEEE) received the B.Sc. degree in electrical engineering from Hohai University, Nanjing, China, in 2019, and the Ph.D. degree in electrical engineering with the School of Electrical Engineering, Southeast University, Nanjing, China, in 2023. He is currently an Assistant Professor with the College of Electrical and Power Engineering, Hohai University. His research interests include the energy storage technology and P2P power transaction.

Jun Liang(Fellow, IEEE) received the B.S. degree in electric power system and its automation from the Huazhong University of Science and Technology, Wuhan, China, in 1992 and the M.S. and Ph.D.degrees in electric power system and its automation from the China Electric Power Research Institute(CEPRI), Beijing, China, in 1995 and 1998, respectively. From 1998 to 2001, he was a Senior Engineer withCEPRI. From 2001 to 2005, he was a Research As sociate with Imperial College London, London, U.K.From 2005 to 2007, he was a Senior Lecturer with the University of Glamorgan.He is currently a Professor in power electronics with the School of Engineering,Cardiff University, Cardiff, U.K. He is the Coordinator and Scientist-in-Charge of two European Commission Marie-Curie Action ITN/ETN projects: MEDOW(€3.9M) and InnoDC (€3.9M). His research interests include HVDC, MVDC,FACTS, power system stability control, power electronics, and renewable powergeneration.Dr. Liang is a Fellow of the Institution of Engineering and Technology. He is the Chair of IEEE U.K. and Ireland Power Electronics Chapter. He is an Editorial Board Member of CSEE JPES. He is an Editor for IEEE TRANSACTIONS ONSUSTAINABLE ENERGY.

Xiangkuan Wan received the Bachelor's degree in Electrical Engineering and Automation from Changchun University of Science and Technology in 2019. He is currently pursuing a Master's degree in Electrical Engineering at Hohai University. His research interests include optimal scheduling and the application of deep reinforcement learning in power systems.